ONSET TIME DETERMINATION OF ACOUSTIC AND ELECTROMAGNETIC EMISSION DURING ROCK FRACTURE

G. Niccolini[1], J. Xu[2, *], A. Manuello[2], G. Lacidogna[2], and A. Carpinteri[2]

[1]Division of Mechanics, Istituto Nazionale di Ricerca Metrologica, Torino, Italy

[2]Department of Structural, Geotechnical and Building Engineering, Politecnico di Torino, Torino, Italy

Abstract—We present an application of the Akaike Information Criterion (AIC) for an automatic and accurate determination of the acoustic and electromagnetic emission (AE and EME) onset times. The onset time information is used to derive the time delays between correlated AE and EME events from rock specimens during laboratory fracture experiments. The observed correlation in time between AE and EME events is consistent with EME release during microcrack growth. Relevant load drops are accompanied by AE bursts, expected to be generated during macrocracks propagation.

1. INTRODUCTION

Mechanical energy is stored as elastic energy in rocks under stress conditions. Most of this energy is then released during the main crack propagation, but a relevant part of it is spent before the failure under acoustic and electromagnetic emissions (AE and EME) [1–7].

The AE phenomenon is the spontaneous release of elastic energy in stressed materials or subjected to harsh environment. Microcrack growth produces redistribution of internal stress in the form of transient elastic waves, called acoustic emissions [1–3].

In recent years, there has been an increasing evidence of electromagnetic precursors due to rock microcracking well before the earthquake occurrence, although the EME source mechanism is not yet fully understood. The EME phenomenon in rocks was initially

attributed to the piezoelectric behaviour of some minerals [6, 7], especially quartz, but this mechanism could be active only in rocks containing a substantial amounts of such components.

As recently proposed, microcracking process involves the breaking of a large number of atomic bonds, which is expected to generate unbalanced charge distributions, of opposite sign, on the opposite sides of the microfractures and, consequently, the onset of strong local electric fields. This has been observed in experiments on the breaking of adhesion bonds [8]. As rocks contain micro-cavities with adsorbed gases, it is therefore possible that the breakdown voltage of the gases can be locally exceeded with generation of micro-electrical discharges and EME.

Another mechanism has been suggested [9] which could be effective in rocks with high electrical resistivity. The opposite charges on the two vibrating fracture faces constitute electric dipoles. The resulting damped electrical oscillations will, in turn, give rise to EME. Electrical relaxation times are sufficiently long to allow for the efficiency of the proposed mechanism, where a very large number of oscillating dipoles with limited lifetime is continuously replenished during crack propagation [6, 7].

Simultaneous AE and EME during compression experiments on rock specimens suggests that the arrival time information of these signals can be exploited for microcrack location with potential applications in earthquake monitoring.

Traditionally, picking the signal onset times was carried out by checking the signal traces based on analyst's experience. Nowadays, handling large volumes of digital and real-time data impose less time consuming and equally objective alternatives. Here, the onset of AE and EME signals is determined by modelling the noise and the signal in windows using the Akaike Information Criterion (AIC) with an automatic procedure for signal data processing able to eliminate false or doubtful onset times.

2. BASIC PRINCIPLE OF *AIC* CRITERION

Initially developed to predict the optimal order of the auto-regressive process fitting the time series in seismology [10–14], the AIC criterion can be used to demark the point of two adjacent time series (noise and signal) with different underlying statistics [15–20].

Suppose that a voltage time series $\{x_1, x_2, \ldots, x_n\}$, containing the AE (or EME) signal, is divided in two segments $i = 1, 2$, $\{x_1, x_2, \ldots, x_k\}$ and $\{x_{k+1}, x_2, \ldots, x_n\}$, where k identifies the unknown signal onset time. Both segments are assumed to be two different

pseudo-stationary time series, either modeled as an auto-regressive (AR) process of order M with coefficients $\{a_m^i\}$:

$$x_j = \sum_{m=1}^{M} a_m^i x_{j-m} + e_j^i \quad i = 1, 2, \tag{1}$$

where $j = M + 1, \ldots, k$ for interval $i = 1$ and $j = k + 1, \ldots, n - M$ for $i = 2$.

The model divides either time series into a deterministic and a non-deterministic part e_j^i, the latter assumed to be a white noise. Thus, the time series $\{e_j^i\}$ is a sample of independent and identically distributed random variables, with mean zero, variance σ_i^2 and density function $f(e_j^i) = (\sigma_i 2\pi)^{-1/2} \exp[-(e_j^i/\sigma_i)^2/2]$, to which the maximum-likelihood estimation (MLE) can be applied. Then, we look at the joint density function of all variables $\{e_j^i\}$ — expressed in terms of the observations $\{x_j\}$ by means of Eq. (1) — considered as fixed parameters, whereas the model parameters $\Theta_i = \Theta_i\,(a_1^i, \ldots a_m^i, \sigma_i^2)$ for the i-th interval are allowed to vary freely. In this perspective, the joint density function is the likelihood function L [15–20]:

$$L(\Theta_1, \Theta_2, k, M|x) = \prod_{i=1}^{2} \left(\frac{1}{\sigma_i^2 2\pi}\right)^{n_i/2} \exp\left[-\frac{1}{2\sigma_i^2} \sum_{j=p_i}^{q_i} \left(x_j - \sum_{m=1}^{M} a_m^i x_{j-m}\right)^2\right], \tag{2}$$

where $p_1 = M + 1$, $p_2 = k + 1$, $q_1 = k$, $q_2 = n - M$, $n_1 = k - M$ and $n_2 = N - k - M$.

As it is known, the MLE finds the particular values of the model parameters which make the observed results the most probable or, in other words, which maximize the likelihood function L. Working equivalently with the logarithm of Eq. (2) and searching for the MLE of the model parameters we get:

$$\frac{\partial \ln L\,(\Theta_1, \Theta_2, k, M\,|x)}{\partial \sigma_i} = 0 \quad i = 1, 2, \tag{3}$$

which has the solution:

$$\sigma_{i,\max}^2 = \frac{1}{n_i} \sum_{j=p_i}^{q_i} \left(x_j - \sum_{m=1}^{M} a_m^i x_{j-m}\right)^2 \quad i = 1, 2. \tag{4}$$

Inserting Eq. (4) into Eq. (2) we get the maximized logarithmic likelihood function [18–20]:

$$\ln L\,(\Theta_1, \Theta_2, k, M|x) = -\frac{k-M}{2} \ln \sigma_{1,\max}^2 - \frac{n-k-M}{2} \ln \sigma_{2,\max}^2 + C_1, \tag{5}$$

where C_1 is a constant.

The expression in Eq. (5) is the basis for the Akaike Information Criterion (AIC), in which the AIC function is defined as $AIC = 2P - 2\ln$ (maximized likelihood function), where P is the number of parameters in the statistical model. Generally, a model with minimum AIC value is thought to be most suitable one among the competing models.

Originally this function was designed to determine the optimal order for an AR process fitting a time series. In the current application, the order M of the AR process is fixed, and therefore the AIC function is a measure for the model fit. The point k where AIC is minimized, or L is maximized, determines the optimal separation of the two time series — the first representing noise and the second containing the signal — in the least square sense, and is interpreted as the onset time of the signal. In this sense, the AIC as a function of k is known as AIC picker [18]:

$$AIC(k) = (k - M)\ln\sigma_{1,\max}^2 + [n - k - M]\ln\sigma_{2,\max}^2 + C_2, \quad (6)$$

where C_2 is a constant.

Alternatively, the AIC value can be directly calculated from the signal without dealing with the AR coefficients. As $M \ll n$, Eq. (6) can be simplified [18]:

$$AIC(k) = k\ln(var(x[1,k])) + (n - k - 1)\ln(var(x[1 + k, n])), \quad (7)$$

where k goes through all the signal trace, and var is the sample variance.

As AIC picker finds the onset point as the global minimum, it is necessary to choose a time window that includes only the segment of interest of the signal. If the time window is chosen properly, AIC picker can find the first arrival of the signal (P-wave arrival for AE) accurately. In case of low S/N ratios (as for noisy EM signals) or more seismic phases (as P-wave and S-wave for AE signals) in a time window, global minimum cannot guarantee to indicate the first arrival of the signal. For this reason a pre-selection of this window is necessary to apply the procedure. Here, the onset time is firstly pre-determined using a threshold amplitude level:

$$\left(\sum_{k=i+1}^{10} |x_k|\right)/10 \geq 4\left(\sum_{k=1}^{i} |x_k|\right)/i, \quad (8)$$

The first value for the index k that makes relation (8) fulfilled is named k_0 and it is the first estimation for the onset time. This first estimation is always localized after the actual onset time. Thus, we apply AIC picker to the interval $[1, k_0]$ for a rough determination of the onset

time, k_1. Then, the application of AIC picker to the time window with center in k_1 and width $2(k_1 - k_0)$ gives the value $k_{\min}$, which is regarded as the actual onset time of the analyzed signal.

3. EXPERIMENTAL SET-UP AND RESULTS

We investigated the fracture of two magnetite [21] and two phonolite [22] cylindrical specimens by constant displacement rate ($1\,\mu\text{m/s}$) uniaxial compression testing. The list of analyzed experiments is reported in Table 1.

The AE activity due to micro-crack growth was detected by applying to the specimen surface a piezoelectric (PZT) transducer, sensitive in the frequency range 50–300 kHz, which converts the high-frequency surface movements due to the AE waves propagation into voltage signals [2, 3]. The EME activity from the specimens was detected by a pickup coil of 500 turns of 0.2 mm copper wire, positioned around the specimen (see Figure 1). According to Faraday's law, variations in the magnetic flux throughout this circuit induces a voltage signal [4, 5].

Table 1. Tested materials and test types.

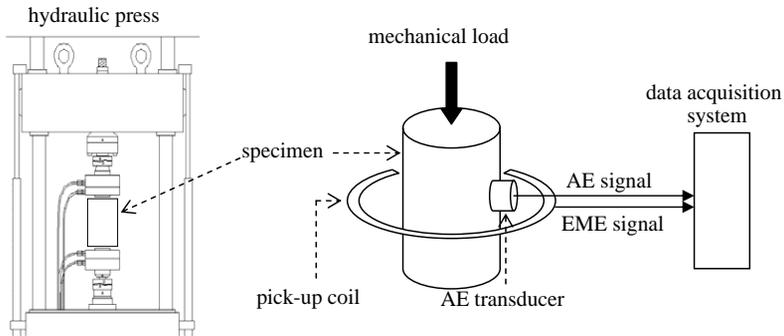| Specimen	Material	Diameter D (mm)	Height H (mm)	Slenderness $\lambda = H/D$	Load (kN)
P1	Magnetite	28	56	2	71.21
P2	Magnetite	28	56	2	47.65
P3	Phonolite	28	56	2	28.81
P4	Phonolite	28	56	2	28.82

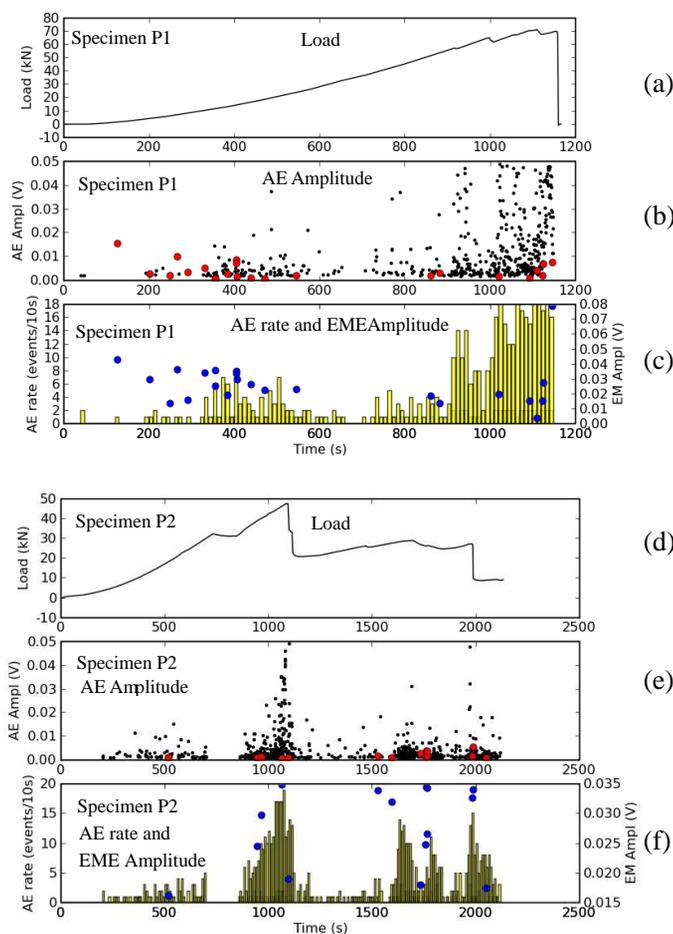**Figure 1.** Schematic representation of the experimental set-up.

Figure 2. (a) Magnetite Specimen P1: load history; (b) AE time series, where red circles mark AE events correlated with EME events; (c) histogram of the AE rate and EME time series; (d) Magnetite Specimen P2: load history; (e) AE time series, where red circles mark AE events correlated with EME events; (f) histogram of the AE rate and EME time series.

As an alternative, the pick-up coil could be situated externally (some centimeters away) of the specimen, with its normal pointing perpendicular or parallel to the specimen axis.

The AE and EME signals were simultaneously recorded by a multi-channel National Instruments digitizer at 1 MSa/s setting a triggered

acquisition. The trigger was set to the AE channel with detection thresholds properly adjusted — from 1 to 2.5 mV for the performed tests — to filter out the noise: thus, no trivial signals were detected before the beginning of the tests. Furthermore, a preliminary fracture test on a wooden block was carried out to verify that none of detected EME pulses may be due to the electronic control system of the testing
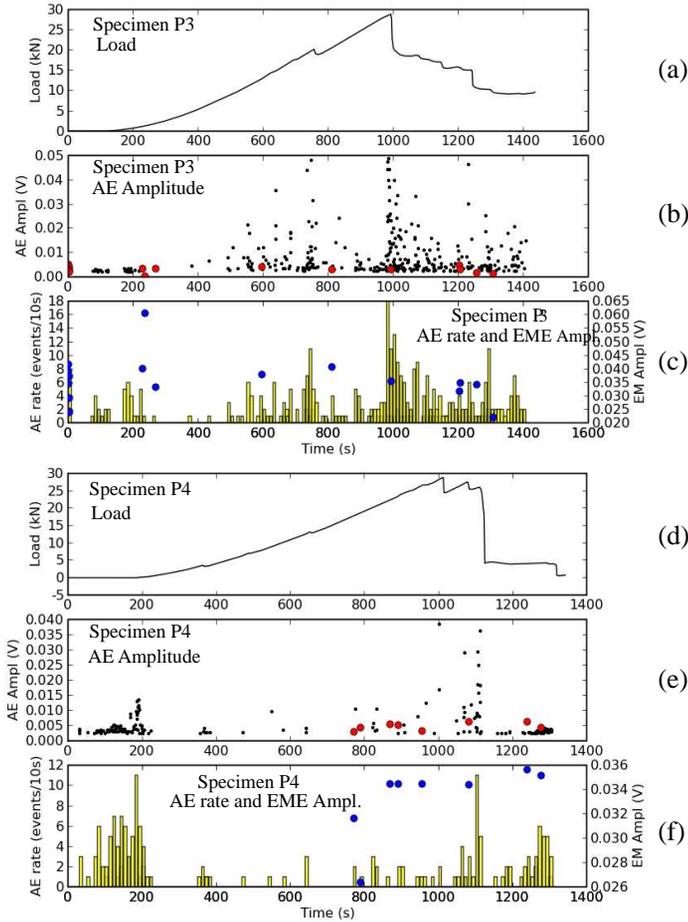

Figure 3. Phonolite Specimen P3: (a load history); (b) AE time series, where red circles mark AE events correlated with EME events; (c) histogram of the AE and EME time series; (d) Phonolite Specimen P4: load history; (e) AE time series, where red circles mark AE events correlated with EME events; (f) histogram of the AE and EME time series.

machine.

For the experiments two specimens were arranged in contact with the press platen with a sheet of Teflon (specimens P1 and P4) and the remaining ones (specimens P2 and P3) without any coupling material, the latter to investigate the influence of triboelectricity produced by friction between the specimen and the press platen on the EME activity. This phenomenon seems to be relevant only for the magnetite specimens (compare Figures 2 and 3).

The load history (Figures 2(a), (d) and 3(a), (d)) and the AE amplitude time series (Figures 2(b), (e) and 3(b), (e)) are plotted for all the specimens, where red circles demark the AE signals simultaneously detected with EME signals. The correlated EME signals, plotted as blue circles, are shown together with the histograms of the AE rate in Figures 2(c), (f) and 3(c), (f).

Both AE and EME signals are represented by the onset time (determined by the *AIC* picker) and the peak amplitude. All tested specimens failed in a brittle manner, i.e., with linear segments of the load-time curve followed by abrupt drops in load-carrying capacity (P1 and P4 are perfectly brittle with a single load drop: see Figures 2(a), 3(d)). Bursts of AE activity containing high-amplitude signals can be clearly correlated with such load drops and are to be considered as signature of crack growth and then as failure precursors (Figures 2(b), (e), and 3(b), (e)).

In the literature it is shown [23–27] that the time for the EME signal to reach the maximum amplitude, T, is related to the crack
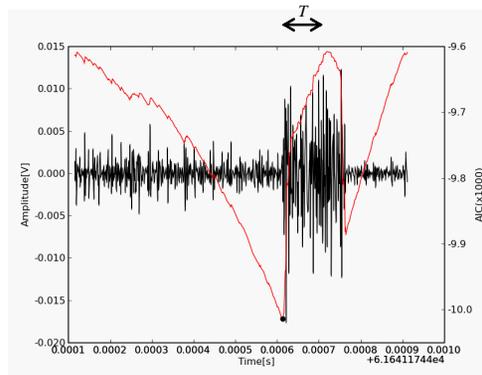

Figure 4. EME signal related to the failure of Magnetite Specimen P2 (occurred at 2000 s since the beginning of test (compare with Figures 2(d)–(f)). Note the time interval $T = 8 \cdot 10^{-5}$ for the EME signal to reach the maximum amplitude.

length, l, by:

$$T = l/v, \tag{9}$$

where v is the crack advancement velocity.

As an example, the estimated length l of main crack developing at the failure time of the Magnetite Specimen P2 is $50\,\text{mm}$, while the measured value of T for the related EME signal (Figure 4) is $8 \cdot 10^{-5}\,\text{s}$. Inserting these values in Eq. (9) results in estimated crack velocity $v = 625\,\text{m/s}$. This value is comparable with ones observed during compressional loading of glass ceramics [24].

Figure 5 shows the onset time $t_{\text{AE(EME)}}$ of an AE (EME) signal trace as the global minimum of the AIC function. Thus, the time delay between correlated AE and EME signals is given by $\Delta t \equiv t_{\text{AE}} - t_{\text{EME}}$. The obtained time delays are not strictly consistent with the hypothesis of AEs and EMEs simultaneously generated by microcracking events. In that case, assuming instantaneous propagation of the EME signals, the time delay may be estimated by $\Delta t = d/v_{AE} \approx 25\,\mu\text{s}$, where $v_{AE} \approx 4 \times 10^3\,\text{ms}^{-1}$ is the speed of sound in the material and $d = 10^{-1}\,\text{m}$ is the specimen size, in contrast with the experimental evidence. In fact, as some of the observed time delays agree with the theory, others are one order of magnitude higher (hundreds of microseconds) or even negatives (the AE precedes the EME wave). The unexpected results for the arrival time delays between time-correlated AE and EME signals may also imply the existence of a non-trivial triggering mechanism of EME by the AE phenomenon.
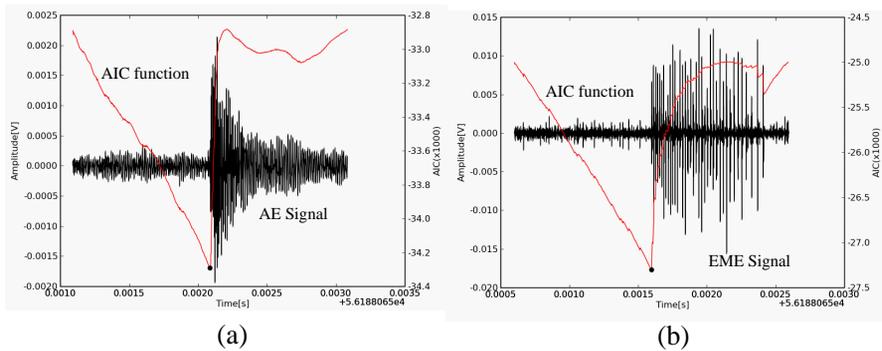

Figure 5. Minimum of the AIC function (red line) identifying the onset time of (a) AE, and (b) EME correlated signals.

4. CONCLUSION

The onset of AE and EME signals from rock fracture is determined through the joint auto-regressive modelling of the noise and the signal, and the application of the Akaike Information Criterion (AIC) using the onset time as parameter. This so-called AIC picker is able to find accurately the onset of genuine signals against the background noise. The presented study suggests the use of EME measurements to enhance monitoring systems based on the AE technique, especially applied to micro-seismicity with potential applications in earthquake forecasting.

The sporadic occurrence of EME events may be due to the experimental settings, with data acquisition triggered by the AE channel, and especially to the reduced width of the investigated EME frequency band (0–500 kHz). Development of measurement methods for EME signals over a broad-band spectrum with high resolution frequency detail, i.e., extending up to some GHz, is necessary to improve the EME statistics for crack location purposes. Furthermore, it would be helpful to use a high-sensitivity centimetric loop as a magnetic sensor. Establishing the time hierarchy between AE and EME correlated events — crucial for understanding their origin and mutual influence — remains an issue under investigation.

REFERENCES

1. Scholz, C. H., "Microfracturing and the inelastic deformation of rock in compression," *J. Geophys. Res.*, Vol. 73, 1417, 1968.
2. Carpinteri, A. and G. Lacidogna, "Damage monitoring of an historical masonry building by the acoustic emission technique," *Materials and Structures (RILEM)*, Vol. 39, 161, 2006.
3. Carpinteri, A., G. Lacidogna, and G. Niccolini, "Critical behavior in concrete structures and damage localization by Acoustic Emission," *Key Eng. Mat.*, Vol. 312, 305, 2006.
4. Lacidogna, G., A. Carpinteri, A. Manuello, G. Durin, G. Niccolini, and A. Agosto, "Acoustic and electromagnetic emissions as precursor phenomena in failure processes," 2010, Strain doi: 10.1111/j.1475-1305.2010.00750.x.
5. Carpinteri, A., G. Lacidogna, A. Manuello, G. Niccolini, A. Schiavi, and A. Agosto, "Mechanical and electromagnetic emissions related to stress-induced cracks," *Experimental Techniques*, Vol. 36, No. 3, 53, 2012.
6. Warwick, J. W., C. Stoker, and T. R. Meyer, "Radio emission

associated with rock fracture: Possible application to the great chilean earthquake of May 22, 1960," *J. Geophys. Res.*, Vol. 87, 2851, 1982.

7. Matsuda, T., C. Yamanaka, and M. Ikeya, "Behavior of stress-induced charges in cement containing quartz crystals," *Phys. Stat. Sol. A*, Vol. 2, 359, 2001.

8. Klyuev, V. A., A. G. Lipson, Y. P. Toporov, A. D. Aliev, A. E. Chlyk, and B. V. Deriaghin, "Charactericescoye islucenye pri rasruscenii tverdikh tel i naruscenii adgesionni sviasei b vacuume," *Dokl. Acad. Nauk SSSR*, Vol. 279, 415, Russia, 1984.

9. Mognaschi, R. and U. Zezza, "Detection of electromagnetic emissions from fracture of rocks and building stones under stress," *5th International Congress on Restoration of Architectural Heritage*, 553–562, Florence 2000.

10. Sleeman, R. and T. van Eck, "Robust automatic P-phase picking: An on-line implementation in the analysis of broadband seismogram recordings," *Physics of the Earth and Planetary Interiors,* Vol. 113, 265, 1999.

11. Earle, P. and P. M. Shearer, "Characterization of global seismograms using an automatic-picking algorithm, *Bull. Seismol. Soc. Am.*, Vol. 84, 366, 1994.

12. Tong, C. and B. L. N. Kennett, "Automatic seismic event recognition and later phase identification for broadband seismograms," *Bull. Seismol. Soc. Am.*, Vol. 86, 1896, 1996.

13. Withers, M., et al., "A comparison of select trigger algorithms for automated global seismic phase and event location," *Bull. Seismol. Soc. Am.*, Vol. 88, 95, 1998.

14. Anant, K. S. and F. U. Dowla, "Wavelet transform methods for phase identification in three-component seismograms," *Bull. Seismol. Soc. Am.*, Vol. 87, 1598, 1997.

15. Kurz, J., C. Grosse, and H. Reinhardt, "Strategies for reliable automatic onset time picking of acoustic emissions and of ultrasound signals in concrete," *Ultrasonics*, Vol. 43, 538, 2005.

16. Zhang, H., C. Thurber, and C. Rowe, "Automatic P-wave arrival detection and picking with multiscale wavelet analysis for single-component recordings," *Bull. Seismol. Soc. Am.*, Vol. 93, 1904, 2003.

17. Hafez, A. G., T. A. Khan, and T. Kohda, "Clear P-wave arrival of weak events and automatic onset determination using wavelet filter banks," *Digital Signal Proc.*, Vol. 20, 715, 2010.

18. Akaike, H., "A new look at the statistical model identification,"

Trans. Automat. Contr., Vol. 19, 716, 1974.

19. Yokota, T., S. Zhou, M. Mizoue, and I. Nakamura, "An automatic measurement of arrival time of seismic waves and its application to an on-line processing system," *Bull. Earthq. Res. Inst.*, Vol. 55, 449, 1981.

20. Maeda, N., "A method for reading and checking phase times in auto-processing system of seismic wave data," *Zisin*, Vol. 38, 365, 1985.

21. Verkaeren, J. and P. Bartholomè, "Petrology of the San Leone magnetite skarn deposit (S. W. Sardinia)," *Economic Geology*, Vol. 74, 53, 1979.

22. Santi, P., et al., "Leucite phonolite millstones from the Orvieto production centre: New data and insights into the roman trade," *Periodico di Mineralogia*, Vol. 73, No. 3, 57, 2004.

23. Frid, V., J. Goldbaum, A. Rabinovitch, and D. Bahat, "Depolarization in percussion drilling of Solenhofen limestone," *J. Appl. Phys.*, Vol. 97, 014908-1, 1997.

24. Frid, V., A. Rabinovitch, and D. Bahat, "Crack velocity measurement by induced electromagnetic radiation," *Phys. Lett. A*, Vol. 356, 160, 2006.

25. Arrighetti, W., P. DeCupis, and G. Gerosa, "Electromagnetic radiation from moving fractal sources: A plane-wave spectral approach," *Progress In Electromagnetics Research*, Vol. 58, 1–19, 2006.

26. Pirhadi, A. and M. Hakkak, "An analytical investigation of the radiation characteristics of infinitesimal dipole antenna embedded in partially reflective surfaces to obtain high directivity," *Progress In Electromagnetics Research*, Vol. 65, 137–155, 2006.

27. Chen, Z. and K.-M. Huang, "Using the oscillating dipoles model to study the electromagnetic radiation induced by fracture of rocks," *Progress In Electromagnetics Research M*, Vol. 14, 221–231, 2010.